Design and manufacturing of permanent magnet bearing rings for high speed applications

Tan Tan [a], Daniel F. Förster [a], Ulrich Pabst [a], Stephan Polachowski [a], Michael Butzek [a], Ghaleb Natour [a, b]

a Central Institute of Engineering, Electronics and Analytics –Engineering and Technology (ZEA-1), Forschungszentrum Jülich GmbH
52425 Jülich, Germany, t.tan@fz-juelich.de
b Faculty of Mechanical Engineering, RWTH Aachen University, 52056 Aachen, Germany

Abstract

We provide an overview of the challenges for the design of magnet rings for high-speed permanent magnet bearings focusing on manufacturing aspects. We analyze an assembly of a NdFeB magnet ring with a hub and a bandage, both made of Ti-6Al-4V (titanium grade 5). Thereby, we consider bandage thicknesses, tolerances and assembling processes. This is supported by simulations using Finite Element Method (FEM) analysis in ANSYS workbench 2020. We analyze the stresses during a press-fit joining process between the magnet and the bandage and subsequent consequences for the stresses on the system for rotation speeds up to 120,000 RPM. Finally, we consider safety aspects by implementing a cracking of the magnet at high rotation speed.

The results of the simulations show that the stresses on the magnet are the limiting factor of the rotation speed in all cases analyzed here. For an idealized system, mainly the bandage thickness and the required rotation speed define suitable tolerances for the fitting of the bandages and magnets. For a real system, residual stresses of the joining process and ovalization effects of the bandage decrease either the allowable speed or the allowable tolerances, thereby considerably influencing the required manufacturing precision. A safety analysis shows that the hub-magnet-bandage assemblies analyzed here are safe with respect to magnet cracking even at high speed.

Keywords: *permanent magnet bearing rings, finite element method, manufacturing and tolerance, fail safe behavior*

1. Introduction

In several cases, special instruments for scientific applications require the use of magnetic bearings. The most common reasons are cases where maintenance is limited or not possible, or where a precision of motion control is required which is only achievable by frictionless bearings. Scientific applications often also demand for highest reliability and compatibility with ultra-high vacuum environments. Radial shear force permanent magnetic bearings (PMBs) with active axial stabilization (Fremerey, 1989) have a relatively low complexity and fulfil these requirements. Thus, they are often used for such purposes, e.g. for choppers and selectors (Cammarata, et al., 2009), (Förster, et al., 2015). The ever-increasing demands of the scientific applications require new optimized PMB designs, especially to achieve very high speeds far beyond 60,000 RPM. As sintered NdFeB magnets have a low tensile strength of only 80 to 90 MPa (IEC 60404-8-1:2015), the most crucial point to enable such high speeds using PMBs is the thorough design of the rotating magnet rings with suitable bandages.

There exist several publications which describe and analyze different design of PMBs with respect to the magnetic forces and bearing stiffnesses. While for high speed permanent magnet motors mechanical analysis was published by several authors (Shen, et al., 2022), we were not able to find publications which deal with manufacturing aspects of PMBs with respect to high speed operation.

2. Design of the high-speed permanent magnet bearing rings

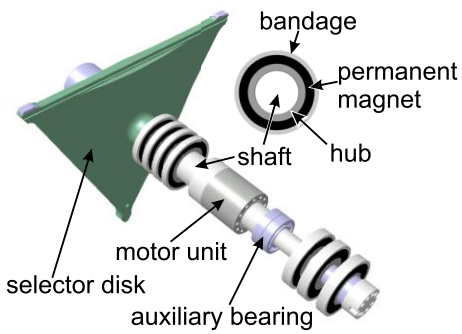

Figure 1 *Rotor of an X-ray pulse selector. The selector disk has a diameter of 194 mm and runs up to 60,000 RPM.*

The considered radial shear force PMBs consist of attractively stacked axially magnetized rings. In the simplest case, such a radial bearing is built by one rotating ring on the shaft and two rings fixed in the housing. The stiffness of such bearings depends on the size and magnetic properties of the magnet rings. It can be considerably increased by using multi-magnet-ring assemblies (Lang and Lembke, 2006). Furthermore, the stiffness can be increased by increasing the amount of the axially stacked magnet rings, i.e. by increasing the axial length of the bearings.

Fig. 1 shows an example rotor of approx. 1 kg mass for an x-ray pulse selector where the main radial bearing consists of stacks of four rotor and four stator magnet rings with a total radial stiffness of about 180 N/mm. The inset in Fig. 1 shows a front view of the magnet ring. The permanent magnets are reinforced by a bandage to withstand the centrifugal load and are mounted on a hub for the fixation to the shaft. These hub-magnet-

bandage assemblies are the only rotating parts of these PMBs. Thus, their design is defining the maximum permissible speed.

Therefore, we investigate the design of the hub-magnet-bandage assemblies with the focus on their mechanical stability. We analyze by the aid of FEM analysis (I) the load at high speeds (up to 120,000 RPM), (II) the manufacturing process to find the necessary interference fit considering manufacturing tolerances, and (III) the fail-safe behavior in case of a magnet fracture.

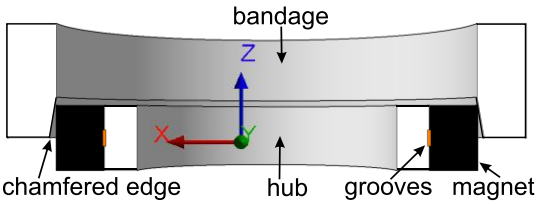

Figure 2 *Cross-sectional view of the hub-magnet-bandage assembly during the axial press-fit process. The orientation of the coordinate system of the simulations is indicated for comparison, y-axis pointing towards the reader.*

The assembling starts at the hub-magnet interface. Between hub and magnet, a low clearance fit H5/h5 is used and the gap is filled with epoxy resin. In the magnet and hub surface, 1 mm wide and 0.2 mm deep grooves are cut facing each other (compare Fig. 2). Filled with epoxy resin, these grooves considerably increase the mechanical interlocking against axial displacement.

For the contact between the bandage and the magnet ring, an interference fit is necessary. The required amount of interference for certain rotor speeds will be analyzed in section No. 4. To assemble interference fit parts, typically shrink-fitting or press-fitting is used.

Shrink fitting is problematic in this case due to the properties of NdFeB magnets. First, the thermal expansion of magnetically oriented NdFeB magnets is anisotropic. It is only substantial in the easy magnetization axis. For directions perpendicular to the easy magnetization axis, the thermal expansion coefficient is very low or even negative (Kumar, et al., 2021). Thereby, the details of the thermal expansion behavior depend on the exact composition of the magnet and the details of the manufacturing process (Rabinovich, et al., 1996). In consequence, cooling of the magnet cannot be considered as a suitable method to shrink the diameter of an axially magnetized NdFeB magnet ring.

Second, the magnet material is heat sensitive and without shrinkage of the magnet it would be necessary to heat up the bandage by several hundred K to establish substantial interference. Even if this process would have no influence on the material properties of the bandage, the temperature at the interface to the magnet would be considerably higher than the operating temperature of high remanence NdFeB magnets. This imposes the risk of partial demagnetization of the magnet in the vicinity of the contact surface.

As a consequence, press-fitting is chosen and further analyzed in detail. To enable the assembling, the bandage is manufactured with a larger axial length and equipped with a chamfered edge (compare Fig. 2). After the bandage is completely pressed onto the magnet, the excess part of the bandage with the chamfered edge is removed by further machining.

The magnet rings for the rotor shown in Fig. 1 have an inner diameter of 26 mm, an outer diameter of 34 mm and an axial length of 4 mm. The related hub-magnet-bandage assemblies are qualified for operation up to 60,000 RPM. By using an improved multi-magnet-ring stator design, it is possible to achieve a similar bearing stiffness for a reduced size of the rotor magnets with an inner diameter of 20 mm, an outer diameter of 26 mm, thereby considerably reducing the centrifugal load on the magnet material. Thus, in the following we use this magnet size for the hub-magnet-bandage assemblies and their optimization for highest possible speeds.

3. Details of the simulation model

The simulation is carried out in Ansys workbench 2020 using purely elastic material models. We use 2D models for the press-fitting process between bandage and magnet considering different interferences. To investigate the bandage ovalization and cracked magnets, 3D models are used. For all simulations, we define frictional contacts between the outer surface of the magnet ring and the inner surface of the bandage. As friction coefficients we chose 0.1 as we assume a lubricated joining process. All other contacts are defined as bonded.

Due to the expected high mechanical load we use titanium grade 5 as bandage material for our simulations. Thus, we can assume that the round bars for manufacturing the bandages have at least an 0.2% offset yield strength of $R_{p0.2}$ = 828 MPa (ASTM B348/B348M-19). For simplicity, we use the same material for the hub.

4. 2D Simulation for magnet ring with interference fit

As starting point, we investigate only the influence of prestress for the hub-magnet-bandage assemblies using 2D simulation. Therefore, we built an ideal model without considering any influence of joining, manufacturing tolerance, and magnet ring defect. We simulate the assembly with different outer diameters from 29 mm (1.5 mm bandage thickness, interference 70 µm), 30 mm (2 mm; 60 µm), 31 mm (2.5 mm; 55 µm) and 32 mm (3 mm; 50 µm) while maintaining a similar joint pressure. Due to the low tensile strength for sintered NdFeB magnets, the stresses in the tension-sensitive

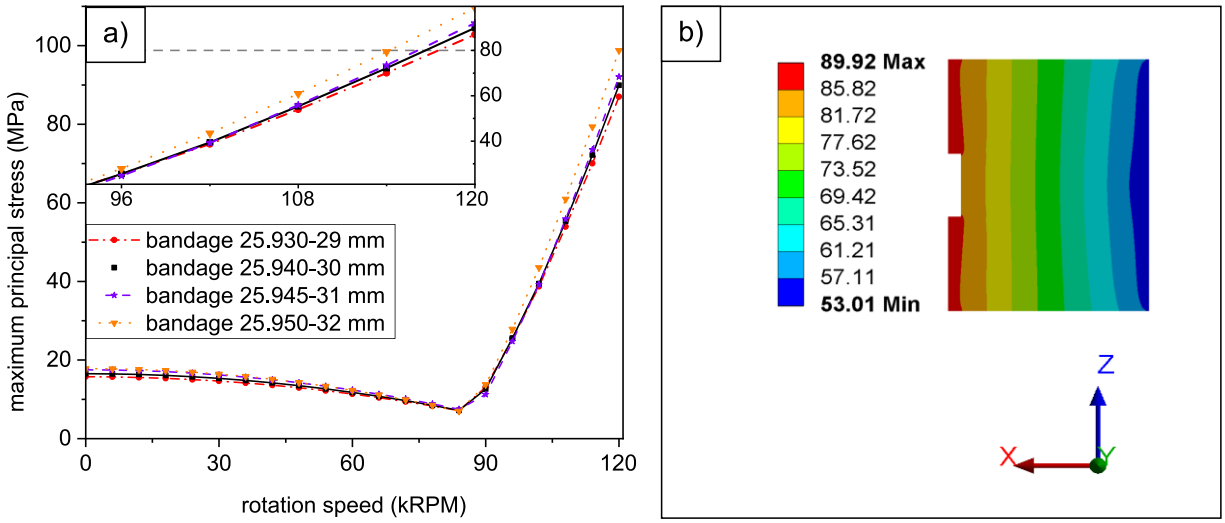

Figure 3 *a) Rotation speed dependent maximum principal stresses of the magnet ring with different bandage outer diameters (2D simulation). The inset is a zoom into the high-speed region. b) Distribution of the maximum principal stress for the magnet ring at 120,000 RPM for the bandage with diameter 25.94-30 mm, color scale given in MPa (2D simulation). The coordinate system is indicated, y-axis pointing towards the reader (compare to Fig. 2).*

magnet rings are the limiting factors for the permissible rotation speed of the hub-magnet-bandage assemblies, as will be shown later on. Hence, we focus here only on the differences in the magnet stresses.

The simulation results in Fig. 3a show that the maximum achievable speed decreases with increasing bandage thickness. Furthermore, for thinner bandages the maintained joint pressure requires larger interferences which increases the acceptable tolerance window. These effects make thinner bandages preferable, whereby the lower thickness limit would be given by the stress inside the bandage as the strain increases because of the larger interferences.

However, there is another effect which has to be considered and which increases with decreasing bandage thickness. Form manufacturing experience we know that relief of internal stresses leads to an ovalization when the bandage is cut off after lathing. This effect is more pronounced for thinner bandages and analyzed further in Sec. 6 using 3D simulations. As consequence, we have chosen 2 mm as bandage thickness for all further simulations, although a thinner bandage would be preferable with respect to the maximum achievable speed and the acceptable tolerance window for manufacturing.

The course of the maximum principal stress in Fig. 3a can be understood considering the different directions of the stresses inside the magnet. Under joint pressure the magnet is radially compressed, leading to axial strain due to the Poisson effect. The subsequent tensile stresses in axial direction reach their maximum at the 1 mm wide grooves. This contribution is highest at zero speed and decreases with increasing speed due to the reduction of the joint pressure. To the contrary, the tangential stresses (in circumferential direction) are initially compressive but increase fast with increasing speed, becoming tensile and the dominant contribution above 84,000 RPM. Fig. 3b shows the distribution of the maximum principal stress for the magnet ring for the final simulation step at 120,000 RPM. The maximum is located in the area of the inner edge.

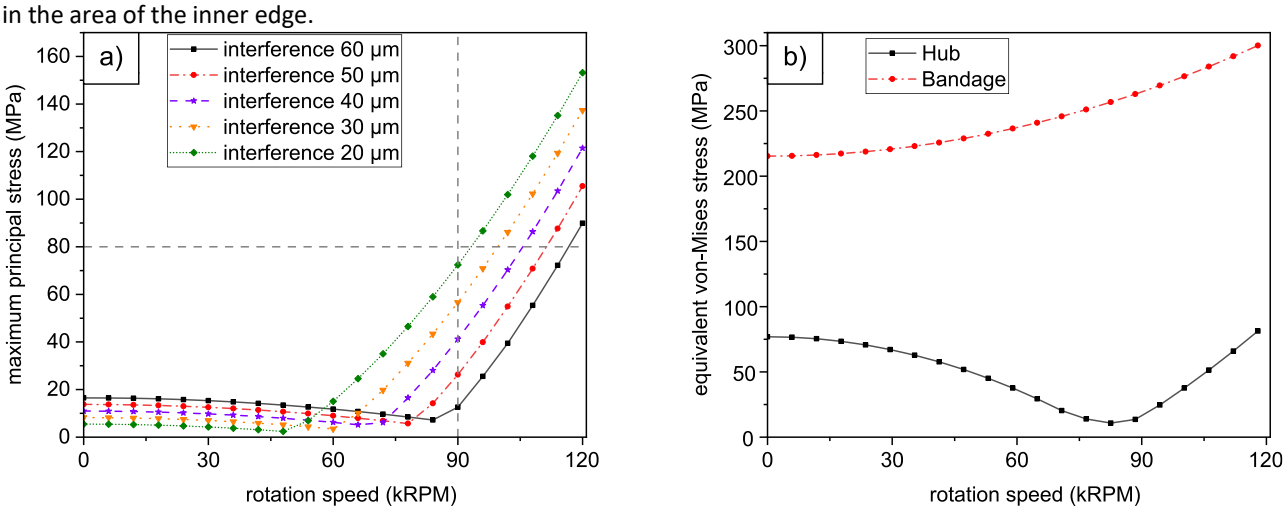

Figure 4 *a) Rotation speed dependent maximum principal stresses of the magnet ring for different interferences between 20 µm and 60 µm (2D simulation). b) Equivalent von-Mises stresses of hub and bandage for 2 mm bandage thickness and 60 µm interference (2D simulation).*

To analyze suitable tolerance windows for manufacturing, we calculate the maximum principle stresses also for lower interferences of 20, 30, 40, and 50 µm as shown in Fig. 4a. Interestingly, if 80 MPa would be used as tensile stress limit for the magnet, the permissible speed for 60 µm interference would be 114,000 RPM and every reduction of the interference by 10 µm would result in a reduction of the permissible speed of about 6,000 RPM.

As mentioned above, the load on bandage and hub are uncritical for all analyzed cases. For example, Fig. 4b shows the equivalent von-Mises stress on hub and bandage for 2 mm bandage thickness and 60 µm interference. Considering $R_{p0.2}$ = 828 MPa and a safety factor of 2 for ductile materials (Rennert, et al., 2012), the stresses remain well below the safety limit.

5. Simulation of joining process

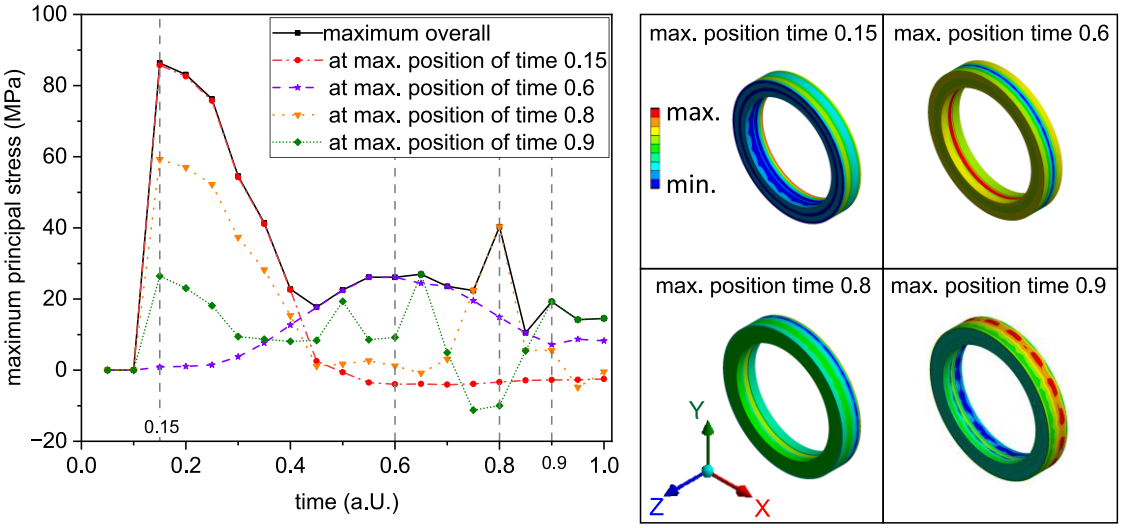

Figure 5 *Maximum principal stress on the magnet ring for 2 mm bandage thickness and 60 µm interference (3D Simulation) and local max. stresses in the magnet ring during the joining process. The orientation of the coordinate system of the simulations is indicated.*

As explained in Sec. 2, we use press-fitting to assemble the bandage on the magnet ring. To avoid damages to the magnet during assembling we also analyze this joining process by simulations. Fig. 5 shows the resulting maximum principal stress on the magnet ring. The black line represents the course of the absolute maximum during the joining process which requires press-forces up to 1260 N. For better understanding of these stress changes during joining, we investigate the four different local max. stresses.

The color-coded magnet rings in Fig. 5 visualize the different max. positions of the stresses. For simplified viewing, we use the results of 3D simulations which we have implemented for the following sections and which lead to similar results as the 2D simulations. For better orientation, the coordinate system is indicated.

Initially, when the magnet is compressed by the bandage at the frontside, the max. stresses occur at the backside of the magnet at the inner edge (time 0.15). At this position, the stress reaches the highest value during the joining process. But later it relaxes here and remains at a low level (red dash-dotted line). At simulation time 0.4 the position of the maximum changes to the inside of the groove (purple dashed line) where it reaches the max. at time 0.6. When the stress relaxes at this position, the maximum changes again to the outer edge of the magnet's backside (time 0.8). At time 0.9, the max. stress is distributed at the outer diameter of the magnet's backside half (close to the excess part of the bandage), but remains at relatively low levels.

After the press-fitting is completed, the simulation continues with the removal of the excess part of the bandage with the chamfered edge. After this step, the stress at the outer diameter relaxes and the maximum is again located at the groove region (not shown).

When the simulation is continued with rotation after the joining process, there are considerable differences to the idealized system discussed in Sec. 4. As can be seen in Fig. 6a, the maximum principal stress is initially slightly lower than for the ideal case, but the fast increase starts about 12,000 RPM earlier. The reason for this behavior is a strong asymmetry of the tangential stresses. Fig. 6b shows the minimum principal stress in the magnet ring after joining, which is solely compressive and oriented in the tangential direction (y-axis of the simulation coordinate system). As remainder

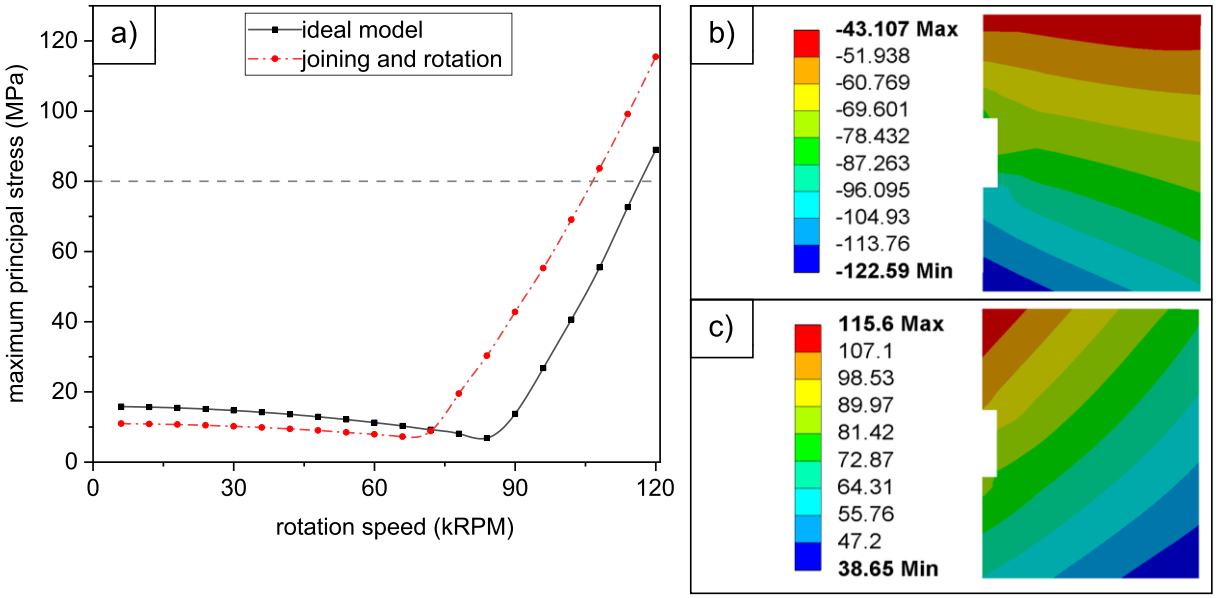

Figure 6 *a) Rotation speed dependent maximum principal stresses of the magnet ring after joining compared with the ideal model. b) Distribution of the minimum principal stress on the magnet ring after joining. c) Distribution of the maximum principal stress on the magnet ring at 120,000 RPM. All results for 2 mm bandage thickness and 60 µm interference. Color scales of 2D simulations given in MPa (compare to Fig. 3b).*

of the joining process, the tangential stress is considerably higher (less compressive) at the frontside (at the top of the image) of the magnet, where the press-fitting process started. This asymmetry is partially conserved with increasing speed and a difference of about ± 25 MPa between frontside and backside remains at 120,000 RPM as can be seen in Fig 6c (compare to Fig. 3b). Please note, that the maximum principal stress in Fig. 6c is tensile and solely oriented in tangential direction.

Again, the stresses in hub and bandage are well below the safety limit for all conditions. The max. equivalent von-Mises stress for the hub is 190 MPa and occurs during the joining process while it is 312 MPa for the bandage at 120,000 RPM.

6. Manufacturing tolerances: bandage ovalization

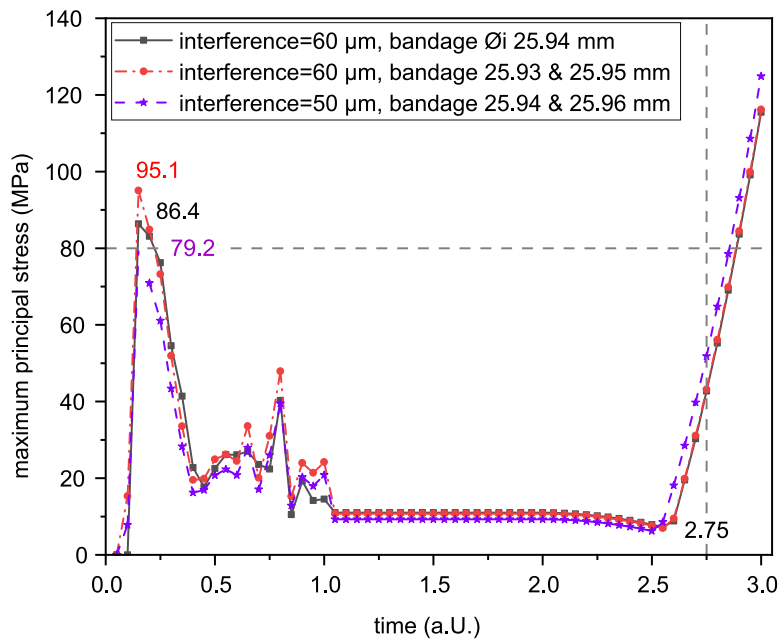

Figure 7 *Maximum principal stress on the magnet ring during the joining process and subsequent rotation for 2 mm bandage thickness and 60 µm interference (black line), 60 µm interference with 10 µm ovalization (dash-dotted red line) and 50 µm interference with 10 µm ovalization (dashed purple line).*

As already mentioned in Sec. 4, the bandage ovalizes when it is cut off after lathing due to internal stress relieve. This causes a circumferential asymmetry of the pressures during the joining process. To estimate possible effects, we simulate the joining process also for a slightly elliptically shaped bandage. Therefore, we model an elliptically shaped interference with a major axis of 70 µm and a minor axis of 50 µm (considered as 60 µm interference with 10 µm ovalization) for comparison with the perfectly circular 60 µm interference. All other parameters remain unchanged.

Fig. 7 shows the maximum principal stress on the magnet ring during the joining process and subsequent rotation for 2 mm bandage thickness and 60 µm interference for a perfectly circular bandage (black line) and for 10 µm ovalization (dash-dotted red line). The stress maximum increases from 86 MPa to 95 MPa, which is above the max. magnet's tensile strength of 90 MPa. To compensate for the increased pressure maximum, the interference can be reduced. For example, the dashed purple line shows

the resulting stresses for a reduced interference of 50 µm, again with 10 µm ovalization. The stress maximum decreases from 95 MPa to 79 MPa. This comes to the cost of increased stress during rotation.

While the ovalization does not significantly influence the stresses during rotation, the reduced interference shifts the fast stress increase during rotation to lower rotation speeds. Thus, due to the necessity of countermeasures to compensate higher joining stresses, ovalization leads to a reduction of the permissible speed for the magnet. For hub and bandage, the max. equivalent von-Mises stresses only increase slightly due to ovalization by approximately 3 % at joining and at 120,000 RPM (for interference 60 µm with 10 µm ovalization). Thus, they remain still well below the safety limit for all conditions.

7. Fail-safe behavior

As part of the safety analysis of the high speed magnetic bearing a failure analysis of the hub-magnet-bandage assemblies is performed. While hub and bandage are made of a ductile metal alloy and are stressed well below their margin of safeties, the tensile stress limit of the magnet is already exceeded at some points of the simulations. Due to the brittle nature of the material, the possibility of undetected magnet defects due to manufacturing flaws or local damage during the joining process requires an analysis for the outcome of magnet cracking at high speed, even for a proper design with a sufficient margin of safety for the tensile magnet stresses.

To simulate the crack in the magnet, we separate the magnet ring in two parts and set bonded connections between them. We define the point of time when the magnet ring cracks and then delete one bonded connection in an additional simulation step. For example, we simulate a crack for a hub-magnet-bandage assembly with 60 µm magnet-bandage interference at 90,000 RPM. With a tensile stress of 43 MPa, the stress on the magnet can be considered to be within the margin of safety for the magnet and thus the corresponding hub-magnet-bandage assembly as suitable for continuous operation at this speed. Due to the crack, the maximum principal stress on the undamaged part of the magnet ring increases only marginally by less than 1 MPa. For the hub, the equivalent von-Mises stress increases after cracking from 41 MPa to 72 MPa. And for the bandage, it increases from 277 MPa to 287 MPa. Thus, all stress increase after cracking is uncritical. As there is also still a contact pressure between bandage and magnet of 27 MPa, the assembly will be held together and can be considered as safe with respect to magnet cracking at the rated operation speed.

8. Conclusion and Outlook

We elucidate several manufacturing-relevant aspects of hub-magnet-bandage assemblies for high-speed permanent magnet bearings. The results of the FEM simulations show that the stresses on the magnet are the limiting factor of the rotation speed in all cases. Remaining stresses of the press-fit joining process and ovalization effects of the bandage decrease allowable tolerances, thereby considerably influencing the required manufacturing precision. A safety analysis shows that the hub-magnet-bandage assemblies remain intact if the magnet cracks at high speed.

For a better understanding of the joining process, we will complement the simulation results by measurements. We will determine the coefficient of friction for unlubricated joining, lubricated joining and joining with adhesive by measuring the pressing force during joining. We will also make microsections of magnets and bandages before and after joining to determine changes of the roughnesses at the contact surfaces and analyze consequences of localized tensile stress above the magnet's strength limit during the press-fitting. Finally, we will perform simulations and experiments for bandages made of carbon fiber-reinforced polymers.

References

ASTM B348/B348M-19 (2019) Standard Specification for Titanium and Titanium Alloy Bars and Billets.

Cammarata M, Eybert L, Ewald F, Reichenbach W, Wulff M, Anfinrud P, Schotte F, Plech A, Kong Q, Lorenc M, Lindenau B, Raebiger J, and Polachowski S (2009) Chopper system for time resolved experiments with synchrotron radiation. Review of Scientific Instruments 80: 015101.

Förster DF, Lindenau B, Leyendecker M, Janssen F, Winkler C, Schumann FO, Kirschner J, Holldack K, and Föhlisch A (2015) Phase-locked MHz pulse selector for x-ray sources. OPTICS LETTERS 40(10): 2265–2268.

Fremerey JK (1989) Radial shear force permanent magnet bearing system with zero power axial control and passive radial damping. In: Schweitzer G (ed) Magnetic Bearings, Springer-Verlag, pp. 25-31.

IEC 60404-8-1:2015 (2015) Magnetic materials - Part 8-1: Specifications for individual materials - Magnetically hard materials.

Kumar R, La Rocca A, Vakil G, Gerada D, Gerada C, and Fernandes BG (2021) Significance of Anisotropic Thermal Expansion in High Speed Electric Machines Employing NdFeB Permanent Magnets. Energies 14: 7558.

Lang M and Lembke TA (2006) Design of Permanent Magnet Bearings with high stiffness. In: ISMB10, 10th International Symposium on Magnetic Bearings, Martigny, Switzerland, 1–4 August 2006, pp. 1–4.

Rabinovich YM, Sergeev VV, Maystrenko AD, Kulakovsky V, Szymura S, and Bala H (1996) Physical and mechanical properties of sintered NdFeB type permanent magnets. Intermetallics 4: 641-645.

Rennert R, Kullig E, Vormwald M, Esderts A, and Siegele D (2012) Rechnerischer Festigkeitsnachweis für Maschinenbauteile aus Stahl, Eisenguss und Aluminiumwerkstoffen. In: FKM-Richtlinie, 6. überarbeitete Auflage, Frankfurt: VDMA-Verlag.

Shen Q, Zhou Z, Liao X, Wang T, He X, and Zhang J (2022) Design and Analysis of the High-Speed Permanent Magnet Motors: A Review on the State of the Art. Machines 10: 549.